Scanning Tunneling Microscopy and X-ray Photoelectron Spectroscopy Studies of Graphene Films Prepared by Sonication-Assisted Dispersion

Elena Y. Polyakova (Stolyarova),[†,*] Kwang Taeg Rim,[‡] Daejin Eom,[§] Keith Douglass,[⊥] Robert L. Opila,[∥] Tony F. Heinz,[§] Andrew V. Teplyakov,[⊥] and George W. Flynn[‡]

[†]Graphene Laboratories Inc, Reading, Massachusetts 01867, United States, [‡]Department of Chemistry and Nanoscale Science and Engineering Center, Columbia University, 3000 Broadway, MC 3109 New York, New York 10027, United States, [§]Department of Physics and Nanoscale Science and Engineering Center, Columbia University, 3000 Broadway, MC 3109 New York, New York 10027, United States, [⊥]Department of Chemistry and Biochemistry, University of Delaware, Newark, Delaware 19716, United States, and [∥]Department of Materials Science and Engineering, University of Delaware, Newark, Delaware 19716, United States

ABSTRACT We describe scanning tunneling microscopy and X-ray photoelectron spectroscopy studies of graphene films produced by sonication-assisted dispersion. Defects in these samples are not randomly distributed, and the graphene films exhibit a "patchwork" structure where unperturbed graphene areas are adjacent to heavily functionalized ones. Adjacent graphene layers are likely in poor mechanical contact due to adventitious species trapped between the carbon sheets of the sample.

KEYWORDS: graphene · sonication-assisted dispersion · scanning tunneling microscopy · X-ray photoelectron spectroscopy

Graphene, a two-dimensional carbon crystal, is a new addition to the family of nanoscale carbon materials.[1,2] It has a unique set of physical properties[3−5] and is being considered for potential use in many practical applications such as graphene-based electronics,[1] optical transistors,[6] liquid crystal[7] and electromechanical devices,[8] chemical[9] and biological sensors,[10] solar batteries,[11,12] micro-electro-mechanical systems (MEMS) and nano-electro-mechanical systems (NEMS),[13] and energy storage,[14] to name a few.

Repeatable and reliable production of nanomaterials is a well-recognized technological challenge. For this reason, large-scale production of high-quality graphene represents a critical step for commercialization of this novel material.[15] In most experiments reported so far, graphene has been produced by mechanical exfoliation.[16−18] This method produces graphene films of excellent crystalline quality,[19] but the yield of thin graphene sheets is extremely low, and the technique cannot be adapted for industrial use.

An active search for alternative methods of graphene production is underway. Very recently, macroscopic scale, high-quality graphene films have been made through several alternative, scalable, and cost-effective methods. First, graphene layers can be grown on top of a metal and later transferred to the desired substrate.[20−22] This method relies on thermally induced epitaxial growth of graphene on a SiC surface[23−27] or chemical vapor deposition (CVD) growth of graphene by decomposition of hydrocarbons on transition metal surfaces[20,22,28] at elevated temperatures. Second, graphene can be produced by chemical splitting of graphite, an abundantly available material.[15,29−31] Initially, a graphite crystal is oxidized and split into soluble graphene oxide (GO).[32] GO can be either restacked as a durable, flexible, nonconducting transparent GO paper[11,33] or reduced back to conductive graphene.[31,34] Such chemically converted graphene sheets can be deposited on virtually any substrate and processed by standard nanofabrication techniques. Several variations of this technique have been reported recently by multiple research groups.[35−37] Unfortunately, the observed resistivity of reduced RO films is too high for many practical applications.

Alternatively, graphite can be split into thin graphene pallets in the liquid phase by sonication of graphite crystals in organic solvent.[7] Such sonication-assisted dispersion methods are inexpensive, straightforward, and, as a result, extremely attractive for industrial production of graphene coatings. However, sonication is a relatively harsh process that might cause high local

* Address correspondence to elena.polyakova@graphenelab.com.

Received for review April 29, 2010 and accepted July 1, 2011.

Published online July 01, 2011
10.1021/nn1009352

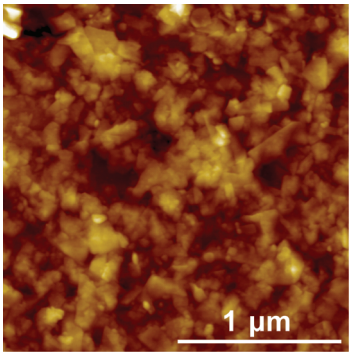

Figure 1. Typical AFM image of a continuous graphitic conductive film prepared by sonication-assisted dispersion. Individual graphene flakes overlap. The image size is 1.8 μm × 1.8 μm.

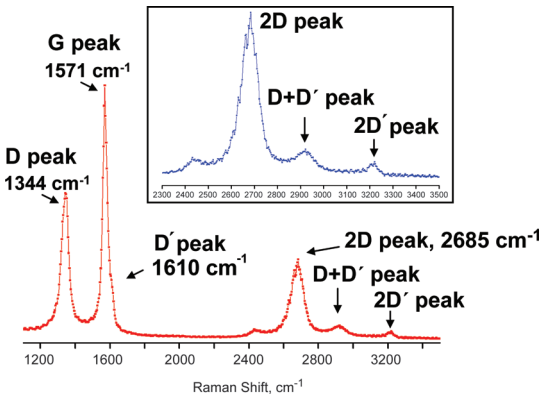

Figure 2. Raman spectrum of a graphene film prepared by sonication-assisted dispersion. The inset shows second-order Raman peaks. The doublet structure of the 2D peak is missing, indicating turbostratisity of the film.

temperatures and pressures with resulting dissociation of molecules in solution.[38] The conductivity of graphene has been found to decrease upon sonication treatment, presumably due to the introduction of defects in the sample, even though no direct chemical treatment is involved in this preparative method.[7] Moreover, in-plane functionalization is critical for effective suspension of graphene films in solution, as unfunctionalized graphene platelets tend to agglomerate, forming graphitic slurries.[39] To date, there is only limited understanding of the nature and origin of the disorder introduced in graphene films by sonication. The present work provides visualization of the atomic structure as well as a quantitative XPS analysis of the chemical composition of ultrathin graphene films prepared by sonication-assisted dispersion.

The samples for this study were supplied by the Manchester group, and the procedure used for preparation of ultrathin graphene films by sonication-assisted dispersion has been described in a previous publication by this group.[7] A brief summary of sample preparation is given in the Materials and Experimental Methods section.

A typical atomic force microscopy (AFM) image of such a film is shown in Figure 1. Individual flakes with surface areas in the range 0.001−0.1 μm^2 can be observed. AFM investigation shows that during spray deposition graphene sheets self-assemble in a continuous thin film with root mean square (rms) size Sq (nm) = 6.74 ± 0.98 . The vast majority of the graphene flakes comprising the film have their basal planes aligned with the substrate surface. AFM images show no wrinkles or out-of-plane edges. A similar process has been previously utilized to prepare graphene oxide membranes[40] and paper.[41] Clustering of this kind is also exhibited by carbon nanotubes that tend to form bundles due to strong van der Waals attraction between the walls of neighboring tubes.[42]

Raman microscopy provides a fast, nondestructive way to measure graphene thickness,[43] as well as to monitor chemical changes[44] and structural damage[45] in various carbon materials. The Raman spectrum of the sample studied here is shown in Figure 2 and provides a signal averaged over an area of ~1 μm^2. A 20% variation in the relative intensities of spectral lines has been observed for Raman spectra collected over randomly selected areas of our sample. Raman spectra routinely collected on a single layer graphene flake have only two prominent features: a first-order G band near 1581 cm^{-1} and a 2D line near 2680 cm^{-1}. The spectrum shown in Figure 2, on the other hand, has a rich structure typical of disordered carbon material in which the sp^2 character of local carbon bonding is partially lost.[45,46]

In particular, the D′ band appears on the blue side of the G band, and several second-order bands, such as 2D, D+D′, and 2D′, are observed. (See inset, Figure 2.) The intensity of these second-order bands is substantially lower than that of the first-order ones, as would be expected for disordered sp^2 carbon films.[45,47] All spectral lines have contributions from several overlapping flakes and are significantly broadened when compared to their counterparts recorded on mechanically exfoliated graphene and graphite.[48] However, the observed Raman lines are sharper than the identical ones in samples of heavily functionalized films such as graphene oxide and reduced graphene oxide.[34,44,47] Raman spectra similar to those reported here have been observed for hydrogenated graphene[49,50] and graphite intercalation compounds in which guest species are found between most of the graphene planes.[51] All these observations suggest that local disorder has been introduced into the graphene planes as a result of sonication.

The shape of the 2D peak is also known to be a sensitive probe of the stacking disorder in graphitic materials.[52] This peak forms as a result of a two-photon resonant process and has a sharp single peak for single-layer graphene. In multilayer graphene, due to splitting of the electronic band structure, the 2D lines take on a complex shape that evolves as a function of

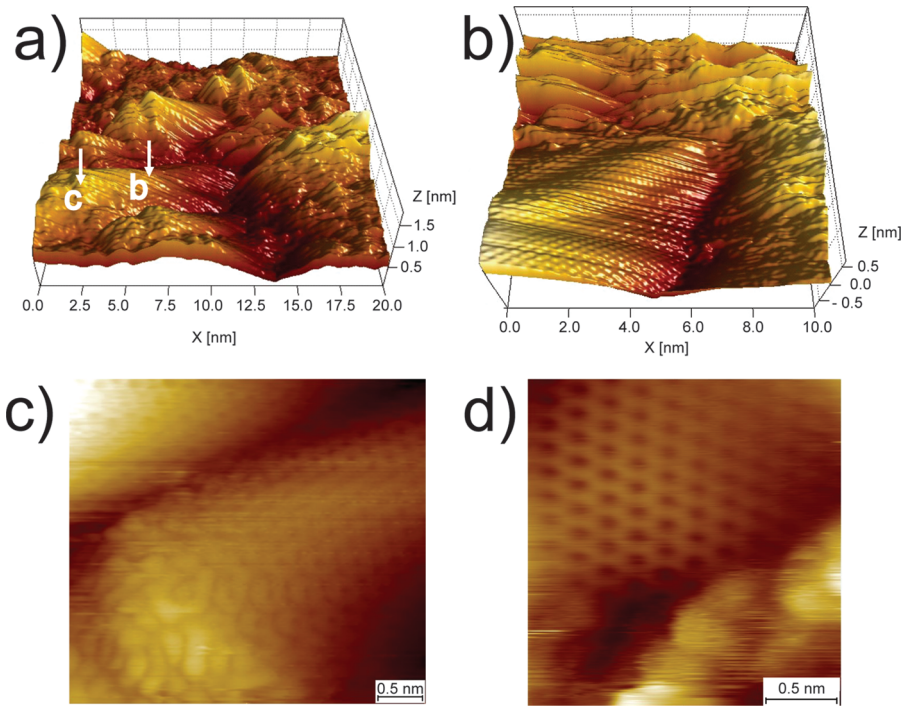

Figure 3. (a) 3D STM topographic image of a 20 nm × 20 nm area for the graphene film. Note the strong local bending of graphene. Arrows point at the center of the enlarged image shown in parts b and c. (b) 3D STM image of 10 nm × 10 nm area for the film from the center of part a. A symmetrical hexagonal pattern is resolved in the lower left corner, while other areas do not show any resolved atomic scale structure. (c) STM image of superstructure near an isolated defect in the lower left corner of part a, for a sample prepared by sonication-assisted dispersion. (d) High-resolution STM image of a border between "perfect" and "functionalized" regions of a graphene film prepared by sonication-assisted dispersion.

the number of layers.[45] In a graphite crystal with an unperturbed ABAB stacking sequence along the *c*-direction of the bulk material, the 2D line has a characteristic doublet shape.[43] The doublet structure of the 2D peak reported for HOPG graphite and thick graphene flakes is lost for turbostratic (disordered along the *c*-axis) graphite. Furthermore, Raman spectra of folded graphene samples with different stacking order, in which two single graphene planes are positioned one on top of the other in a random orientation, exhibit a 2D line with a single peak. In the present samples the 2D line has a complex shape with maximum intensity near 2670 cm^{-1} (see Figure.2, inset). This line contains contributions from many one- and few-layer thick graphene flakes, making a unique assignment of the Raman peaks difficult. The absence of graphite-like doublet structure suggests that no ABAB stacking of graphene flakes occurs during spray deposition of the film and that graphene flakes are randomly rotated with respect to each other.

To further analyze the sample, atomically resolved images of graphene films were obtained using scanning tunneling microscopy (STM) under UHV conditions at 77 K, following experimental procedures descried elsewhere.[19,53] Scanning conditions were $V_{bias} = -1$ V, $I_{tun} = 1$ nA. Images were collected in six different randomly chosen spots separated by hundreds of micrometers; no significant differences were found between STM images recorded in these widely separated areas. A typical topographic STM image on the 20 nm × 20 nm scale (Figure 3a) reveals strong local buckling. No Moiré structures, which would be expected for two graphene sheets rotated at an arbitrary angle and positioned one on top of the other,[54] were observed. An expanded view of the area centered at the position marked by arrows in Figure 3a is shown in Figure 3, parts b and c. A hexagonal pattern, which is similar to that reported for graphene on a Si/SiO_2 wafer,[19,55] appears at the lower left corner (Figure 3d), while no resolved atomic image could be obtained in the other areas. An important observation is that the structure of the graphene film is not uniform. "Perfect" graphene patches do not exceed 5 nm × 5 nm in size, and neighboring areas are heavily disordered.

STM images are a sensitive gauge of the crystalline quality of graphene films, as local lattice distortion causes the appearance of $\sqrt{3} \times \sqrt{3}$ superstructures. The appearance of superstructure in these images is an electronic effect due to enhancement of tunneling current arising from wave function interference near scattering centers.[56] These superstructures are routinely observed in STM images recorded on graphite surfaces near lattice imperfections such as step edges,[57] nanoscale defects,[58] deposited metal clusters,[59] defects induced by ion bombardment,[60]

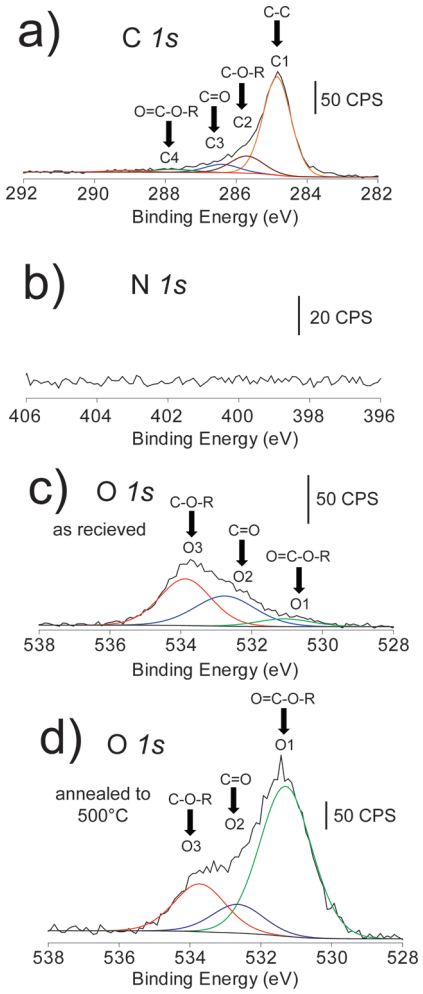

Figure 4. XPS spectra for graphene films prepared by sonication-assisted dispersion. (a) C 1s peak; (b) N 1s peak; (c) O 1s peak; (d) O 1s peak after annealing at 500 °C in UHV.

and strongly absorbed species.[61] Typically, superstructures near point-like defects have distinct 3-fold symmetry, but if the defect extends over several lattice unit cells, irregular features, ranging over distances of 1−5 nm, can appear in the vicinity of the defected area. In our experiments, $\sqrt{3} \times \sqrt{3}$ superstructures were found occasionally near severely buckled areas, such as marked by arrow (c) in Figure 3a and magnified in Figure 3c. Surprisingly, in the majority of recorded images, "perfect" graphene areas were directly adjoined to "functionalized" areas, and no $\sqrt{3} \times \sqrt{3}$ superstructures could be resolved near the border between these two regions (see Figure 3d). This suggests that no nanoscopic scattering defects, such as pits or boundaries, were introduced into the graphene network.

It should be noted that the observed "buckled" topography of sonicated graphene films, which is to be contrasted with the smooth "wavy" landscape found for mechanically exfoliated graphene films mounted on Si/SiO_2 substrate,[19,55] is commonly found in functionalized graphene films. Formation of local bending in a defect-free graphene sheet is energetically unfavorable but can be justified by the breaking of local symmetry through in-plane functionalization.[62]

Since STM is not sensitive to the chemical composition of the sample, further examination of the atomic content and local chemical environment of the elements in the graphene films required the use of X-ray photoelectron spectroscopy (XPS), a surface-sensitive technique that probes the top 3 to 4 nm of a material sample.[63]

Figure 4 summarizes the results of the XPS investigation of graphene samples prepared by sonication-assisted dispersion. The carbon (C 1s), nitrogen (N 1s), and oxygen (O 1s) XPS spectra recorded after preparation and storage under ambient conditions are shown in Figure 4a, 4b, and 4c,d, respectively. The energies of all spectra were calibrated on the basis of setting the C 1s peak for each sample to 284.8 eV.[47] The spectral set presented in Figure 4a−c corresponds to the sample prepared by sonication-assisted dispersion and investigated without any additional treatment. The C 1s spectra (Figure 4a) were fit with up to four peaks using binding energies of 284.8, 285.7, 286.8, and 288.7 eV. These peaks correspond to the following carbon components: C−C (C1), C−O−R (C2), C═O (C3), and O═C−O−R (C4),[47] with epoxide groups (C−O−C) having similar binding energies to those of C−O−R. The C1 peak is attributed to carbon atoms of the unperturbed graphene network. The N 1s spectra show no observable nitrogen. Thus, the DMF solvent used in the sonication-assisted dispersion sample preparation does not bind to the graphene and is effectively removed to a level below the XPS detection limit during film deposition.

We detected a strong feature in the oxygen O 1s region (Figure 4c) that can be fit with three distinct peaks (at 531.0, 532.8, and 533.8 eV) corresponding to likely oxygen-containing species of the type O═C−O−R (O1), C═O (O2), and C−O−R (O3).[47] After annealing the sonication-assisted dispersion sample at 500 °C in UHV the C−C (C1) peak increased slightly in intensity, while the other peaks decreased. Upon this treatment, the relative contributions of O1, O2, and O3 peaks composing the O 1s peak change dramatically (Figure 4d). O1 (O═C−O−R) functionalities, which were only minor contributors to the O 1s spectrum of the untreated sample (Figure 4c), have now become a major spectral component, indicating chemical conversion of oxygen-containing species.

The most striking finding of XPS studies is that the graphene films have very high oxygen content, as no deliberate oxidation is involved in sample preparation. Even though natural graphite crystals often show the presence of a weak oxygen peak in an XPS survey, the observation of a rich oxygen signal is only typical for graphene oxide, which has been subjected to harsh acid treatment in order to separate graphene planes.[64]

The presence of oxygen-containing groups is likely to be enhanced by the well-known ability of graphitic materials to capture and host foreign atoms and molecules, with graphite intercalation compounds[65] as the most vivid example. In loosely packed graphene-based structures, such as the ones under consideration here, pathways for molecular diffusion are available between graphene sheets, resulting in accumulation of adventitious species. Our XPS data show that thermal treatment does not affect most carbon atoms in these samples, but strongly influences oxygen-containing species or compounds, as is expected for interstitial contaminants. Several sources of oxygen, such as absorbed water, partially functionalized hydrocarbons, molecular oxygen, and functional groups attached to the graphene plane, must be considered as the origin of these peaks.

For practical applications such as flexible electronics and touch-screens, it is crucial to reduce the resistivity of graphene coatings. Blake *et al.*[7] observed that the resistance of graphene films prepared by sonication-assisted dispersion at low temperatures deviates from a variable-range-hopping model but can, nevertheless, be described by a simple activation energy dependent process that scales as $\exp(-\Delta/T)$. This low-temperature behavior has been attributed to weak tunnel-like coupling between overlapping flakes. Poor coupling between graphene layers due to impurities trapped between graphene sheets or in-plane graphene functionalization are both consistent with the present observations.

We envision that the conductivity of graphene-based films prepared by this method can be significantly improved if techniques that are milder than sonication, such as careful stirring, are used for graphite sheet separation. In addition, deposition in a controlled water- and oxygen-free environment might be helpful in achieving desirable physical and chemical properties. Another route for the improvement of film quality is co-deposition of graphene flakes with conductive particles, thereby providing more effective electric coupling between adjacent graphene flakes.

In conclusion, we have employed STM, Raman microscopy, and XPS to examine graphene films prepared by sonication-assisted dispersion. As a result of the preparation procedure, graphene films are heavily contaminated by adventitious species, and graphite-like ABAB stacking is not restored during film deposition, which is likely due to the accumulation of impurities between graphene layers.

MATERIALS AND EXPERIMENTAL METHODS

For sample preparation, graphite flakes were sonicated in dimethylformamide (DMF). Following sonication, thick flakes were removed by centrifugation. The remaining suspension was sprayed on a silicon wafer covered by a thermally grown 300 nm oxide layer, preheated to 150 °C. As a result, continuous conductive films, ~1.5 nm thick, were formed on top of the wafer. Up to 50% of the graphene sheets in these films are one atomic layer thick.[7] After preparation, the samples were annealed for 2 h in an atmosphere of argon (90%)/hydrogen (10%) at 250 °C.

AFM images and Raman spectra were collected at Columbia University, and the parameters stated in the text were used. All XPS measurements were performed at the University of Delaware using a PHI-5600 instrument equipped with a monochromated Al Kα excitation source (1486.6 eV) and a hemispherical analyzer positioned at 45° to the sample surface. Curve fitting and percent composition calculations were performed using CasaXPS software.

Acknowledgment. We are indebted to A. Geim and R. Nair for providing samples, and we thank K. Bolotin for stimulating and enlightening discussions. Raman spectra and AFM images were taken at Brookhaven National Laboratory's Center for Functional Nanomaterials, which is supported by the Department of Energy under grant DE-AC02-98CH10886. This work was supported at Columbia University by the National Science Foundation through grant CHE-07-01483 (to G.W.F.), by the National Science Foundation through the NSEC Program (CHE-06-41523), and by the New York State Office of Science, Technology, and Academic Research (NYSTAR). Material support was provided by the U.S. Department of Energy (DE-FG02-88-ER13937 to G.W.F.) and by the Air Force Office of Scientific Research (MURI FA955009-1-0705). At the University of Delaware, this work was supported by the National Science Foundation through grant CHE-0650123 (to A.V.T.) and through IGERT (DGE-0549399).

REFERENCES AND NOTES

1. Geim, A. K.; Novoselov, K. S. The Rise of Graphene. *Nat. Mater.* **2007**, *6*, 183–191.
2. Geim, A. K. Graphene: Status and Prospects. *Science* **2009**, *324*, 1530–1534.
3. Novoselov, K. S.; Geim, A. K.; Morozov, S. V.; Jiang, D.; Zhang, Y.; Dubonos, S. V.; Grigorieva, I. V.; Firsov, A. A. Electric Field Effect in Atomically Thin Carbon Films. *Science* **2004**, *306*, 666–669.
4. Lee, C.; Wei, X.; Kysar, J. W.; Hone, J. Measurement of the Elastic Properties and Intrinsic Strength of Monolayer Graphene. *Science* **2008**, *321*, 385–388.
5. Zhang, Y. B.; Tan, Y. W.; Stormer, H. L.; Kim, P. Experimental Observation of the Quantum Hall Effect and Berry's Phase in Graphene. *Nature* **2005**, *438*, 201–204.
6. Wang, F.; Zhang, Y.; Tian, C.; Girit, C.; Zettl, A.; Crommie, M.; Shen, Y. R. Gate-Variable Optical Transitions in Graphene. *Science* **2008**, *320*, 206–209.
7. Blake, P.; Brimicombe, P. D.; Nair, R. R.; Booth, T. J.; Jiang, D.; Schedin, F.; Ponomarenko, L. A.; Morozov, S. V.; Gleeson, H. F.; Hill, E. W.; *et al.* Graphene-Based Liquid Crystal Device. *Nano Lett.* **2008**, *8*, 1704–1708.
8. Bunch, J. S.; van der Zande, A. M.; Verbridge, S. S.; Frank, I. W.; Tanenbaum, D. M.; Parpia, J. M.; Craighead, H. G.; McEuen, P. L. Electromechanical Resonators from Graphene Sheets. *Science* **2007**, *315*, 490–493.
9. Schedin, F.; Geim, A. K.; Morozov, S. V.; Hill, E. W.; Blake, P.; Katsnelson, M. I.; Novoselov, K. S. Detection of Individual Gas Molecules Adsorbed on Graphene. *Nat. Mater.* **2007**, *6*, 652–655.
10. Mohanty, N.; Berry, V. Graphene-Based Single-Bacterium Resolution Biodevice and DNA Transistor: Interfacing Graphene Derivatives with Nanoscale and Microscale Biocomponents. *Nano Lett.* **2008**, *8*, 4469–4476.
11. Liu, Q.; Liu, Z.; Zhang, X.; Zhang, N.; Yang, L.; Yin, S.; Chen, Y. Organic Photovoltaic Cells Based on an Acceptor of Soluble Graphene. *Appl. Phys. Lett.* **2008**, *92*, 223303.

12. Wang, X.; Zhi, L.; Mullen, K. Transparent, Conductive Graphene Electrodes for Dye-Sensitized Solar Cells. *Nano Lett.* **2008**, *8*, 323–327.
13. Chen, C.; Rosenblatt, S.; Bolotin, K. I.; Kalb, W.; Kim, P.; Kymissis, I.; Stormer, H. L.; Heinz, T. F.; Hone, J. Performance of Monolayer Graphene Nanomechanical Resonators with Electrical Readout. *Nat. Nanotechnol.* **2009**, *4*, 861–867.
14. Stoller, M. D.; Park, S.; Zhu, Y.; An, J.; Ruoff, R. S. Graphene-Based Ultracapacitors. *Nano Lett.* **2008**, *8*, 3498–3502.
15. Ruoff, R. Graphene: Calling all Chemists. *Nat. Nanotechnol.* **2008**, *3*, 10–11.
16. Bolotin, K. I.; Sikes, K. J.; Jiang, Z.; Klima, M.; Fudenberg, G.; Hone, J.; Kim, P.; Stormer, H. L. Ultrahigh Electron Mobility in Suspended Graphene. *Solid State Commun.* **2008**, *146*, 351–355.
17. Han, M. Y.; Ozyilmaz, B.; Zhang, Y. B.; Kim, P. Energy Band-Gap Engineering of Graphene Nanoribbons. *Phys. Rev. Lett.* **2007**, *98*, 206805.
18. Heersche, H. B.; Jarillo-Herrero, P.; Oostinga, J. B.; Vandersypen, L. M. K.; Morpurgo, A. F. Bipolar Supercurrent in Graphene. *Nature* **2007**, *446*, 56–59.
19. Stolyarova, E.; T., R. K.; Ryu, S.; Maultzsch, J.; Kim, P.; Brus, L. E.; Heinz, T. F.; Hybertsen, M. S.; Flynn, G. W. High-Resolution Scanning Tunneling Microscopy Imaging of Mesoscopic Graphene Sheets on an Insulating Surface. *Proc. Natl. Acad. Sci. U. S. A.* **2007**, *104*, 9209–9212.
20. Reina, A.; Jia, X.; Ho, J.; Nezich, D.; Son, H.; Bulovic, V.; Dresselhaus, M. S.; Kong, J. Large Area, Few-Layer Graphene Films on Arbitrary Substrates by Chemical Vapor Deposition. *Nano Lett.* **2009**, *9*, 30–35.
21. Gall, N. R.; Rut'kov, E. V.; Tontegode, A. Y. Two Dimentional Graphite Films on Metals and Their Intercalation. *Int. J. Mod. Phys. B* **1997**, *11*, 1865–1911.
22. Kim, K. S.; Zhao, Y.; Jang, H.; Lee, S. Y.; Kim, J. M.; Kim, K. S.; Ahn, J.-H.; Kim, P.; Choi, J.-Y.; Hong, B. H. Large-Scale Pattern Growth of Graphene Films for Stretchable Transparent Electrodes. *Nature* **2009**, *457*, 706–710.
23. Berger, C.; Song, Z.; Li, X.; Wu, X.; Brown, N.; Naud, C.; Mayou, D.; Li, T.; Hass, J.; Marchenkov, A. N.; *et al*. Electronic Confinement and Coherence in Patterned Epitaxial Graphene. *Science* **2006**, *312*, 1191–1196.
24. Emtsev, K. V.; Speck, F.; Seyller, T.; Ley, L.; Riley, J. D. Interaction, Growth, and Ordering of Epitaxial Graphene on SiC{0001} Surfaces: A Comparative Photoelectron Spectroscopy Study. *Phys. Rev. B* **2008**, *77*, 155303.
25. Emtsev, K. V.; Bostwick, A.; Horn, K.; Jobst, J.; Kellogg, G. L.; Ley, L.; McChesney, J. L.; Ohta, T.; Reshanov, S. A.; Röhrl, S. A. Towards Wafer-Size Graphene Layers by Atmospheric Pressure Graphitization of Silicon Carbide. *Nat. Mater.* **2009**, *8*, 203–207.
26. Tromp, R. M.; Hannon, J. B. Thermodynamics and Kinetics of Graphene Growth on SiC(0001). *Phys. Rev. Lett.* **2009**, *102*, 106104.
27. Sprinkle, M.; Soukiassian, P.; de Heer, W. A.; Berger, C.; Conrad, E. H. Epitaxial Graphene: the Material for Graphene Electronics. *Phys. Status Solidi RRL* **2009**, *3*, A91–A94.
28. Li, X.; Cai, W.; An, J.; Kim, S.; Nah, J.; Yang, D.; Piner, R.; Velamakanni, A.; Jung, I.; Tutuc, E.; *et al*. Large-Area Synthesis of High-Quality and Uniform Graphene Films on Copper Foils. *Science* **2009**, *324*, 1312–1314.
29. Park, S.; Ruoff, R. S. Chemical Methods for the Production of Graphenes. *Nat. Nanotechnol.* **2009**, *4*, 217–224.
30. Li, D.; Muller, B., M.; Gilje, S.; Kaner, R. B.; Wallace, G. G. Processable Aqueous Dispersions of Graphene Nanosheets. *Nat. Nanotechnol.* **2008**, *3*, 101–105.
31. Li, X.; Zhang, G.; Bai, X.; Sun, X.; Wang, X.; Wang, E.; Dai, H. Highly Conducting Graphene Sheets and Langmuir-Blodgett Films. *Nat. Nanotechnol.* **2008**, *3*, 538–542.
32. Hummers, W. S.; Offeman, R. E. Preparation of Graphitic Oxide. *J. Am. Chem. Soc.* **1958**, *80*, 1339.
33. Stankovich, S.; Dikin, D. A.; Dommett, G. H. B.; Kohlhaas, K. M.; Zimney, E. J.; Stach, E. A.; Piner, R. D.; Nguyen, S. T.; Ruoff, R. S. Graphene-Based Composite Materials. *Nature* **2006**, *442*, 282–286.
34. Gómez-Navarro, C.; Weitz, R. T.; Bittner, A. M.; Scolari, M.; Mews, A.; Burghard, M.; Kern, K. Electronic Transport Properties of Individual Chemically Reduced Graphene Oxide Sheets. *Nano Lett.* **2007**, *7*, 3499–3503.
35. Green, A. A.; Hersam, M. C. Solution Phase Production of Graphene with Controlled Thickness via Density Differentiation. *Nano Lett.* **2009**, *9*, 4031–4036.
36. Si, Y.; Samulski, E. T. Synthesis of Water Soluble Graphene. *Nano Lett.* **2008**, *8*, 1679–1682.
37. Gilje, S.; Han, S.; Wang, M.; Wang, K. L.; Kaner, R. B. A Chemical Route to Graphene for Device Applications. *Nano Lett.* **2007**, *7*, 3394–3398.
38. Suslick, K. S.; Flannigan, D. J. Inside a Collapsing Bubble: Sonoluminescence and the Conditions during Cavitation. *Annu. Rev. Phys. Chem.* **2008**, *59*, 659–683.
39. Jang, B.; Zhamu, A. Processing of Nanographene Platelets (NGPs) and NGP Nanocomposites: a Review. *Science* **2008**, *43*, 5092–5101.
40. Chen, C.; Yang, Q.-H.; Yang, Y.; Lv, W.; Wen, Y.; Hou, P.-X.; Wang, M.; Cheng, H.-M. Self-Assembled Free-Standing Graphite Oxide Membrane. *Adv. Mater.* **2009**, *21*, 1–5.
41. Dikin, D. A.; Stankovich, S.; Zimney, E. J.; Piner, R. D.; Dommett, H. B.; Evmemenko, G.; Nguyen, S. T.; Ruoff, R. S. Preparation and Characterization of Graphene Oxide Paper. *Nature* **2007**, *448*, 457–460.
42. Ebbesen, T. W. Carbon Nanotubes. *Annu. Rev. Mater. Sci.* **1994**, *24*, 235–264.
43. Ferrari, A. C.; Meyer, J. C.; Scardaci, V.; Casiraghi, C.; Lazzeri, M.; Mauri, F.; Piscanec, S.; Jiang, D.; Novoselov, K. S.; Roth, S.; *et al*. Raman Spectrum of Graphene and Graphene Layers. *Phys. Rev. Lett.* **2006**, *97*, 187401.
44. Kudin, K. N.; Ozbas, B.; Schniepp, H. C.; Prud'homme, R. K.; Aksay, I. A.; Car, R. Raman Spectra of Graphite Oxide and Functionalized Graphene Sheets. *Nano Lett.* **2008**, *8*, 36–41.
45. Ferrari, A. C. Raman Spectroscopy of Graphene and Graphite: Disorder, Electron-Phonon Coupling, Doping and Nonadiabatic Effects. *Solid State Commun.* **2007**, *143*, 47–57.
46. Ferrari, A. C.; Robertson, J. Resonant Raman Spectroscopy of Disordered, Amorphous, and Diamondlike Carbon. *Phys. Rev. B* **2001**, *64*, 075414.
47. Yang, D.; Valamakanni, A.; Bozoklu, G.; Park, S.; Stoller, M.; Piner, R. D.; Stankovich, S.; Jung, I.; Field, D. A.; Ventrice, C. A., Jr.; *et al*. Chemical Analysis of Graphene Axide Films after Heat and Chemical Treatments by X-ray Photoelectron and Micro-Raman Spectroscopy. *Carbon* **2009**, *47*, 145–152.
48. Yan, J.; Zhang, Y.; Kim, P.; Pinczuk, A. Electric Field Effect Tuning of Electron-Phonon Coupling in Graphene. *Phys. Rev. Lett.* **2007**, *98*, 166802–166804.
49. Elias, D. C.; Nair, R. R.; Mohiuddin, T. M. G.; Morozov, S. V.; Blake, P.; Halsall, M. P.; Ferrari, A. C.; Boukhvalov, D. W.; Katsnelson, M. I.; Geim, A. K.; *et al*. Control of Graphene's Properties by Reversible Hydrogenation: Evidence for Graphane. *Science* **2009**, *323*, 610–613.
50. Ryu, S.; Han, M. Y.; Maultzsch, J.; Heinz, T. F.; Kim, P.; Steigerwald, M. L.; Brus, L. E. Reversible Basal Plane Hydrogenation of Graphene. *Nano Lett.* **2008**, *8*, 4597–4602.
51. Dresselhaus, M. S.; Dresselhaus, G. Intercalation Compounds of Graphite. *Adv. Phys.* **1981**, *30*, 139–326.
52. Wilhelm, H.; Lelaurain, M.; McRae, E.; Humbert, B. Raman Spectroscopic Studies on Well-Defined Carbonaceous Materials of Strong Two-Dimensional Character. *J. Appl. Phys.* **1998**, *84*, 6552–6558.
53. Stolyarova, E.; Stolyarov, D.; Bolotin, K.; Ryu, S.; Liu, L.; Rim, K. T.; Klima, M.; Hybertsen, M.; Pogorelsky, I.; Pavlishin, I.; *et al*. Observation of Graphene Bubbles and Effective Mass Transport under Graphene Films. *Nano Lett.* **2009**, *9*, 332–337.
54. Sinitsyna, O. V.; Yaminsky, I. V. Atomic Resolution Probe Microscopy of the Graphite Surface. *Usp. Khim.* **2006**, *75*, 27–35.
55. Ishigami, M.; Chen, J. H.; Cullen, W. G.; Fuhrer, M. S.; Williams, E. D. Atomic Structure of Graphene on SiO_2. *Nano Lett.* **2007**, *7*, 1643–1648.

56. Magonov, S.; Whangbo, M. *Surface Analysis with STM and AFM: Experimental and Theoretical Aspects of Image Analysis*; VCH Publishers: Weinheim, 1996.
57. Niimi, Y.; Matsui, T.; Kambara, H.; Tagami, K.; Tsukada, M.; Fukuyama, H. Scanning Tunneling Microscopy and Spectroscopy of the Electronic Local Density of States of Graphite Surfaces near Monoatomic Step Edges. *Phys. Rev. B* **2006**, *73*, 085421–085428.
58. Liu, L.; Rim, K. T.; Eom, D.; Heinz, T. F.; Flynn, G. W. Direct Observation of Atomic Scale Graphitic Layer Growth. *Nano Lett.* **2008**, *8*, 1872–1878.
59. Xhie, J.; Sattler, K.; Müller, U.; Venkateswaran, N.; Raina, G. Periodic Charge-Density Modulations on Graphite near Platinum Particles. *Phys. Rev. B* **1991**, *43*, 8917–8923.
60. Shedd, G. M.; Russell, P. E. The Effects of Low-Energy Ion Impacts on Graphite Observed by Scanning Tunneling Microscopy. *J. Vac. Sci. Technol. A* **1991**, *9*, 1261–1264.
61. Kelly, K. F.; Mickelson, E. T.; Hauge, R. H.; Margrave, J. L.; Halas, N. J. Nanoscale Imaging of Chemical Interactions: Fluorine on Graphite. *Proc. Natl. Acad. Sci. U. S. A.* **2000**, *97*, 10318–10321.
62. Schniepp, H. C.; Li, J.-L.; McAllister, M. J.; Sai, H.; Herrera-Alonso, M.; Adamson, D. H.; Prud'homme, R. K.; Car, R.; Saville, D. A.; Aksay, I. A. Functionalized Single Graphene Sheets Derived from Splitting Graphite Oxide. *J. Phys. Chem. B* **2006**, *110*, 8535–8539.
63. Briggs, D.; Seah, M. P. *Practical Surface Analysis, Auger and X-ray Photoelectron Spectroscopy*, 2nd ed.; John Wiley & Sons: New York, 1996.
64. Cai, D.; Song, M. Preparation of Fully Exfoliated Graphite Oxide Nanoplatelets in Organic Solvents. *J. Mater. Chem.* **2007**, *17*, 3678–3680.
65. Enoki, T.; Endo, M.; Suzuki, M., *Graphite Intercalation Compounds and Applications*; Oxford University Press, 2003.